JOURNAL OF MATERIALS SCIENCE 20 (1985) 2702–2710

Multicomponent toughened ceramic materials obtained by reaction sintering

Part 2 *System ZrO_2–Al_2O_3–SiO_2–MgO*

P. MIRANZO, P. PENA, J. S. MOYA, S. DE AZA
Instituto de Cerámica y Vidrio (CSIC), Arganda del Rey, Madrid, Spain

Very dense zirconia–toughened ceramics with a mullite matrix based on the quaternary system ZrO_2–Al_2O_3–SiO_2–MgO in the temperature range as low as 1450 to 1500° C have been obtained by reaction sintering of zircon/alumina/magnesia mixtures. The shrinkage, advance of reaction, microstructure, densification mechanism and mechanical properties are reported. The results are explained in terms of transitory and permanent liquids that appear at $\leqslant$ 1425° C and ~ 1450° C respectively.

1. Introduction

As mentioned in Part 1 of this work [1], reaction sintering between zircon and alumina in order to produce zirconia–toughened mullite has been extensively studied. In this second paper the effect of magnesia addition on the reaction sintering of $ZrSiO_4/Al_2O_3$ mixtures has been investigated.

Taking into account the compatibility relationships of the quaternary system ZrO_2–Al_2O_3–SiO_2–MgO (Fig. 1), as well as the experimental results obtained in previous works [2, 3], we have studied two compositions of $ZrSiO_4/Al_2O_3$/MgO mixture with the following molar proportions: $2ZrSiO_4 + 3Al_2O_3 + x(MgO + Al_2O_3)$, where the x values were 0.3 and 1. These compositions are located in the subsolidus compatibility plane ZrO_2–mullite–spinel; the corresponding invariant point is located at about 1450° C. Reaction sintering takes place according to the following equation:

$$\underset{\text{zircon}}{2ZrSiO_4 + 3Al_2O_3 + x(Al_2O_3 + MgO)} \quad (1)$$

$$\rightleftarrows \underset{\text{mullite}}{2ZrO_2 + Al_6Si_2O_{13}} + \underset{\text{spinel}}{xMgAl_2O_4}$$

From a tentative projection of the primary phase volume of ZrO_2 from the zirconia corner on the opposite face of the composition tetrahedron (Fig. 2) and from the phase evolution observed (Fig. 3) it can be stated that the two compositions considered are located in the primary phase field of ZrO_2, while in the case of the secondary phase it is possible to deduce, with a small margin of error, that for MgO contents higher than 2.5 wt% the secondary phase that appears is Al_2O_3, and for contents lower than this value, the corresponding secondary phase is mullite [2].

2. Experimental procedure

The raw materials used were zircon opacifer supplied by Quiminsa, Spain (Opazir S), a finely milled mineral zircon; Fluka alumina of 99.998 wt% purity; and magnesia prepared by steam-heating magnesium metal millings of 99.96% purity at 2 atm pressure, followed by calcination of $Mg(OH)_2$ product in a platinum dish for 2 h at 1200° C.

The preparation, firing, X-ray analysis, microstructure analysis, dilatometric measurements and mechanical properties were as in Part 1 [1]. Three compositions of $2ZrSiO_4/3Al_2O_3/x(Al_2O_3 + MgO)$ with molar proportion $x = 0$, 0.3 and 1 were studied.

As before, [1] the sample densities were measured by both water and mercury displacement, and theoretical densities were calculated taking into account the product phase compositions together with the true density of zircon, α-alumina, tetragonal zirconia (t), monoclinic zirconia (m), mullite, MgO and spinel, namely 4.68, 3.97, 6.10, 5.83, 3.16, 3.58 and 3.59 Mg m^{-3} respectively.

0022–2461/85 $03.00 + .12

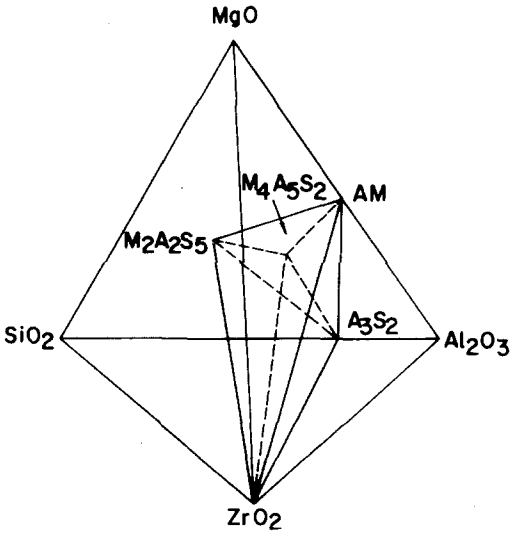

Figure 1 Solid-state compatibility relationships in the ZrO_2–Al_2O_3–SiO_2–MgO system.

3. Results and Discussion

According to the tentative projection of the primary phase volume of zirconia (Fig. 2), it is possible to state that a transient liquid, corresponding to the invariant point where saphirine–spinel–cordierite–zirconia coexist, will appear at temperatures lower than 1400° C. At temperatures below about 1425° C, another transient liquid appears corresponding to the invariant point saphirine–spinel–mullite–zirconia. Finally, at a temperature above about 1450° C the formation of the permanent liquid takes place. Taking into account the above and considering the X-ray diffraction (XRD) patterns of the $x = 1$ sample treated at different temperatures (Fig. 4), it is possible to deduce the following reaction sequence:

$$Al_2O_3 + MgO \xrightarrow{T<1350^\circ C} Al_2MgO_4$$

$$ZrSiO_4 + Al_2MgO_4 + Al_2O_3 \xrightarrow{1350^\circ C<T<1425^\circ C}$$

$$ZrO_2 + Al_2MgO_4 + Al_{10}Mg_4Si_2O_{33} \quad (2)$$

$$+ \text{transient liquid} + (Al_2O_3 + ZrSiO_4)$$

$$\xrightarrow{1425^\circ C<T<1450^\circ C} ZrO_2 +$$

$$+ Al_6Si_2O_{13} + Al_2MgO_4$$

At temperatures below 1350° C there is no liquid phase, consequently Al_2MgO_4 was formed by solid-state reaction as a consequence of its low free energy of formation (Fig. 5).

In Fig. 6 the sample shrinkage $\Delta L/L_0$, where L_0 is the initial length, is plotted as a function of temperature for the three compositions. It can be observed that as the MgO content increased the shrinkage started to be significant at a lower temperature. This temperature was near 1400° C, so temperatures ranging between 1425 and 1500° C were selected. As can be seen in this Figure, the shrinkage for $x = 1$ is lower than for $x = 0.3$ for temperatures between 1300° and 1400° C. This fact can be explained by the formation of an aluminium magnesium spinel, as has been detected by XRD. This is an expansive phase that decreases the overall shrinkage rate of the $x = 1$ sample.

It has been observed [1] in a CaO-containing sample that a transient liquid phase enhances the sintering rate. In the same way, the transient liquids that appear at temperatures below about 1400 and 1425° C can explain the fact that the MgO-containing samples show higher shrinkage rate than that of the composition without MgO addition at a temperature lower than 1450° C. Over the peritectic temperature in MgO-containing samples, the permanent liquid phase appears; consequently a liquid-phase sintering takes place, which produces a change in the slope of the shrinkage curve (Fig. 6).

There are several processes that can lead to the densification of a powder compact. The identification of the controlling mechanism can be a major problem. The $x = 0$ composition is used to elucidate which of the two most important mechanisms, bulk diffusion or grain-boundary diffusion, gives rise to densification.

In the case of solid-state sintering, mathematical models have been constructed to estimate the densification rate and the activation energy of this process by using experimental data [4]. It is possible to assume that the shrinkage from non-isothermal experiments with constant heating rate can be given by the following equation [4, 5]:

$$\left(\frac{\Delta L}{L_0}\right)^n = \left(K_0 R T^2 \frac{n}{Qa}\right) \exp\left(-\frac{Q}{RT}\right) \quad (3)$$

where $K_0 \sim 1/T$, R is the gas constant, Q the activation energy, a the heating rate and n is 2.0 or 3.1 when the densification is controlled by bulk diffusion or grain-boundary diffusion respectively.

Equation 3 was fitted by least-squares and this fit was used for the composition without MgO content for both values of n. For $n = 2.0$ the activation energy was 535 kJ mol^{-1}, while for

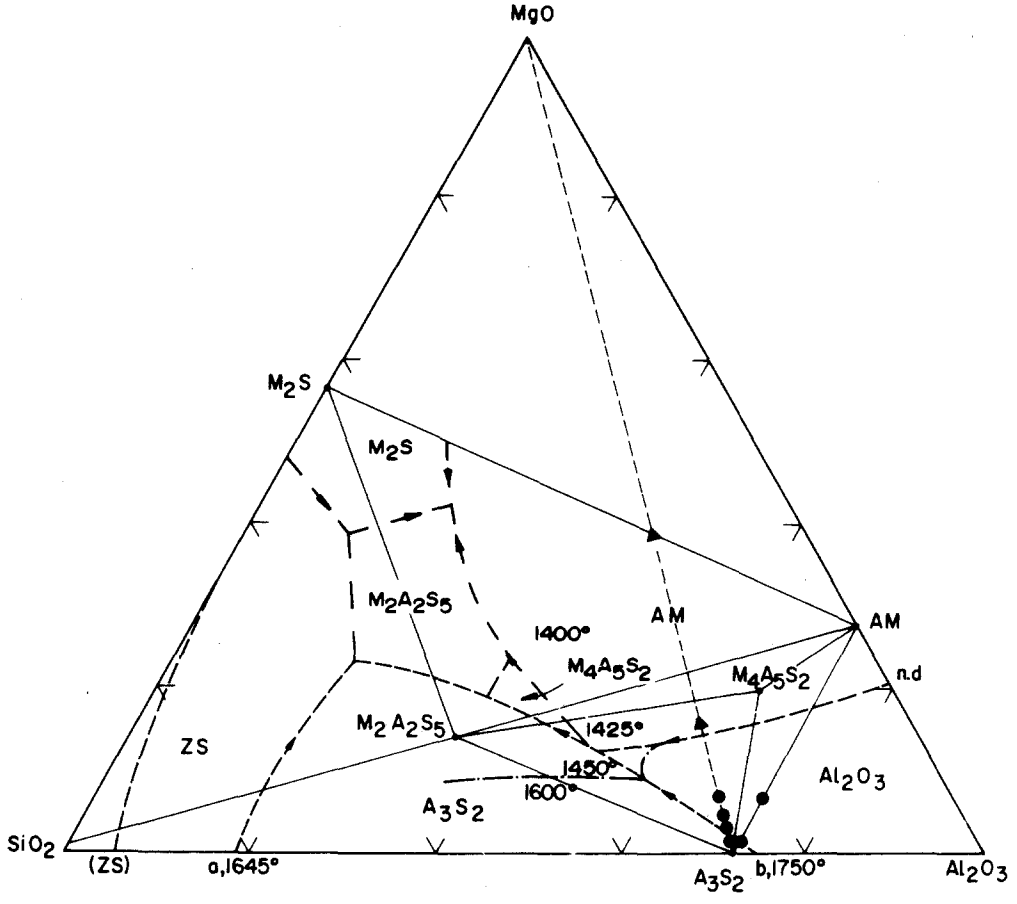

Figure 2 Projection of the primary volume of crystallization of ZrO_2 on the opposite face (Al_2O_3–MgO–SiO_2) of the tetrahedron Al_2O_3–MgO–SiO_2–ZrO_2, showing phase boundaries, isotherms and solid state compatibilities. • present authors, ▲ from [3].

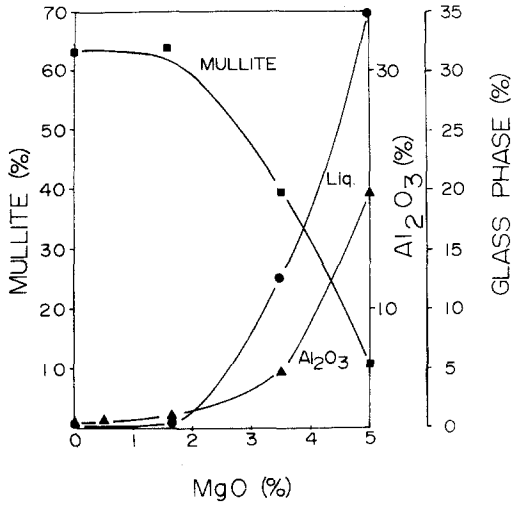

Figure 3 Phase evolution against MgO addition for 10 h at 1600° C.

$n = 3.1$ it was 829 kJ mol^{-1}. Taking into account the value 439 kJ mol^{-1} obtained by Di Rupo Anseau and Brook [6], it is clear that in this case diffusion occurs through the bulk of the sample. This fit and the experimental data have been plotted in Fig. 7.

Fig. 8 shows the evolution of the reaction of Equation 1 for $x = 0$, $x = 0.3$ and $x = 1$ compositions, as well as the densification for $x = 0.3$ and $x = 1$ against time at 1450° C. In this figure it can be observed that (a) the reaction rate is significantly higher in the case of MgO-containing compositions, and this rate increased with MgO content; and (b) in this case $ZrSiO_4$ decomposition and mullite formation, as well as the sintering process, occur simultaneously. At a lower temperature of 1425° C, however, (Fig. 9), $ZrSiO_4$ decomposition occurs prior to mullite formation as observed and discussed in Part 1 [1].

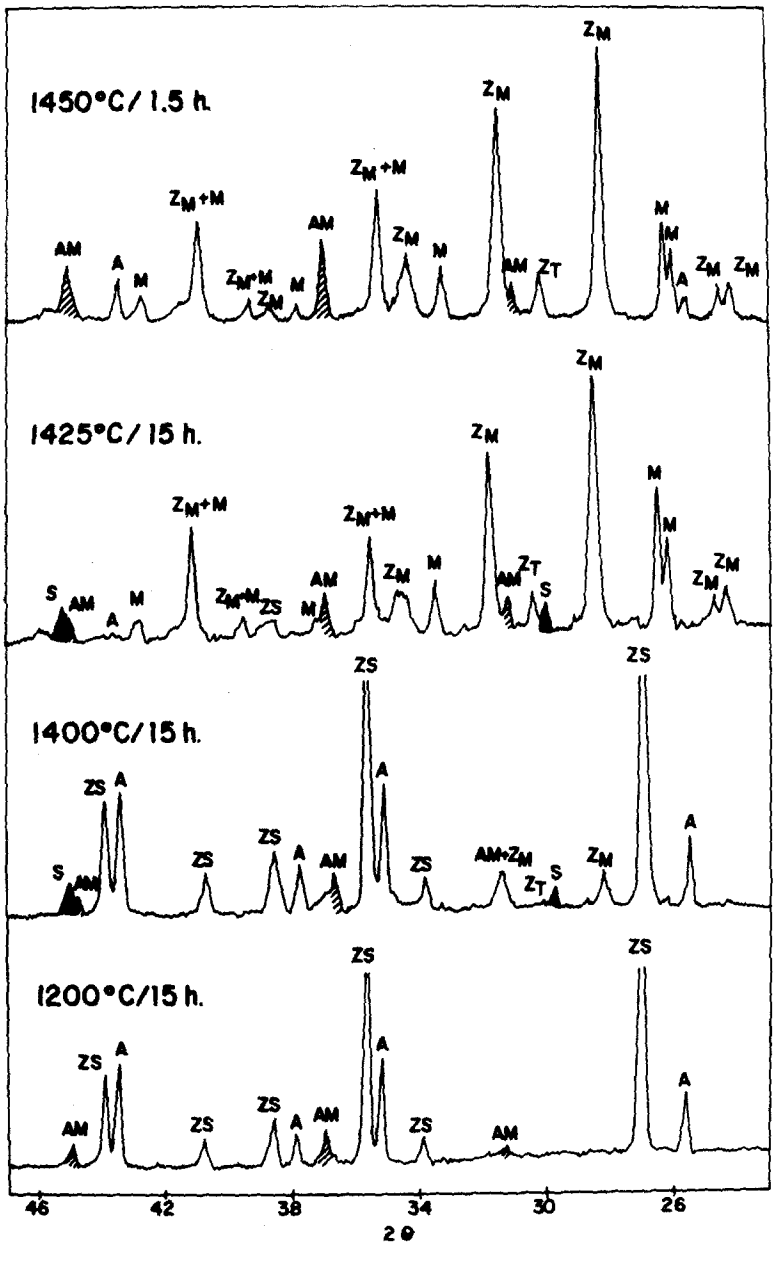

Figure 4 XRD patterns of the $x = 1$ sample treated at different temperatures.

It is clear from Figs. 9 and 10 that the rate of the reaction of Equation 1 is very temperature-dependent. At 1500° C, in the case of $x = 1$, the amount of mullite formed is significantly lower than at 1450 and 1425° C, which is in good agreement with the corresponding quaternary system: for this composition and at this temperature the secondary phase is alumina and not mullite, i.e. at $T > 1450°$ C the mullite will dissolve in a liquid phase and alumina appears.

It is interesting to notice that in the case of MgO-containing samples the reaction rate is higher than in the case of CaO-containing samples for the same temperature interval, i.e. for $x = 1$ at 1425° C the $ZrSiO_4$ decomposition is completed after ~2 h (Fig. 9), while in the case of CaO-containing samples ~30 h are necessary to complete the decomposition of zircon (see Fig. 7 of [1]).

Fig. 11 shows the microstructure of the sample with $x = 1$, treated for 1.5 h at 1450° C. In this photomicrograph it is possible to distinguish two kinds of zirconia particles. One, named *intragranular*, is enclosed in mullite grains and has,

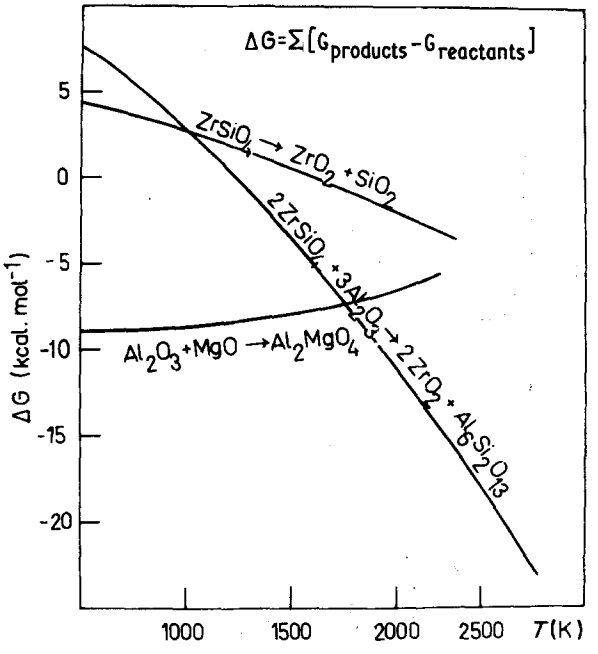

Figure 5 Free energy against temperature for the solid-state dissociation of zircon, and for the solid-state reaction of alumina and magnesia.

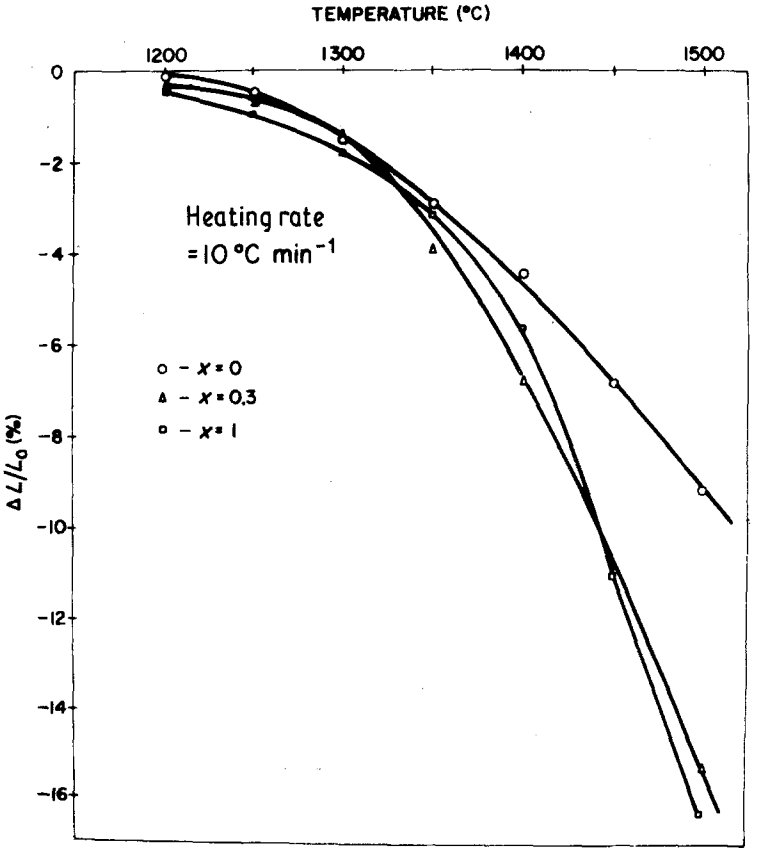

Figure 6 Sample shrinkage against temperature for the three compositions.

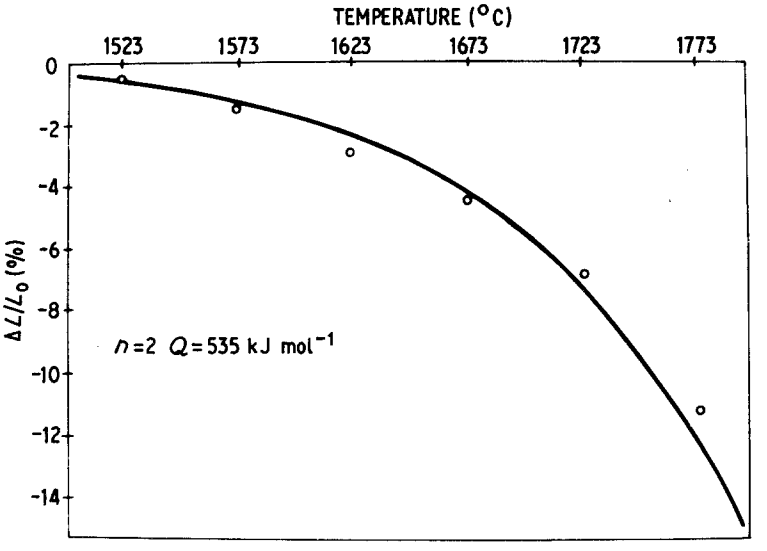

Figure 7 Plot of Equation 3 fitted for the composition without MgO content (solid line), and experimental data (o).

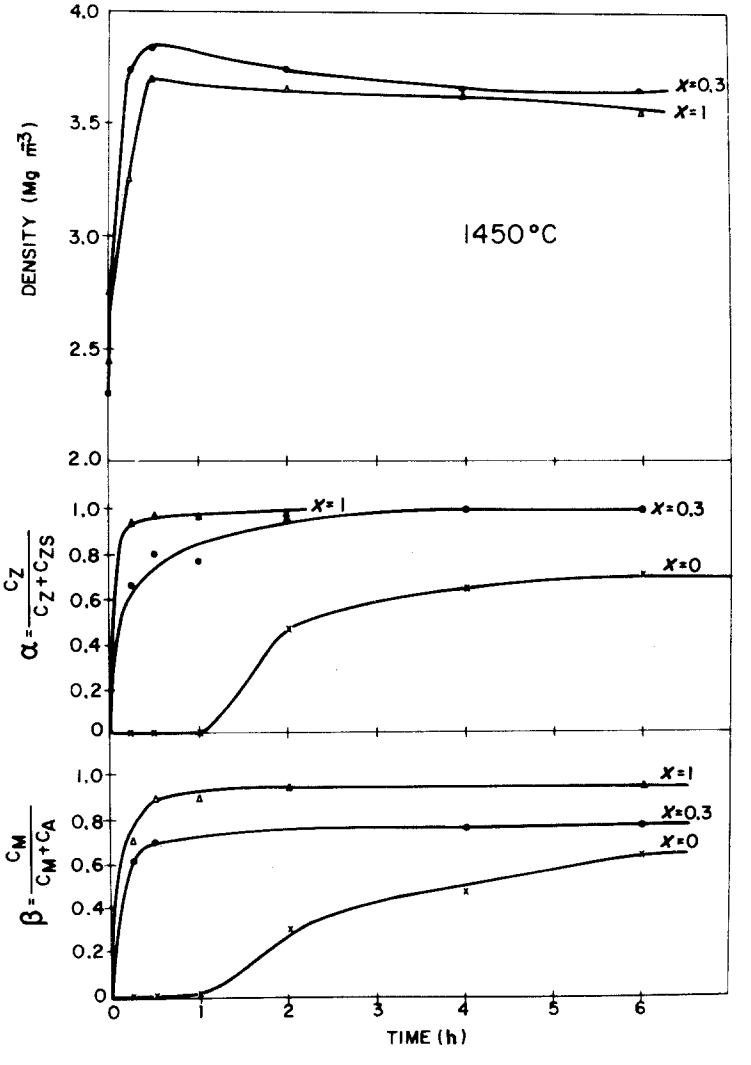

Figure 8 Evolution of the reaction of Equation 1 for $x = 0$, $x = 0.3$ and $x = 1$ as well as densification for $x = 0.3$ and $x = 1$, plotted against time at 1450° C. C_m, C_A, C_z, C_{zs} are the concentration of mullite, alumina, zirconia and zircon respectively.

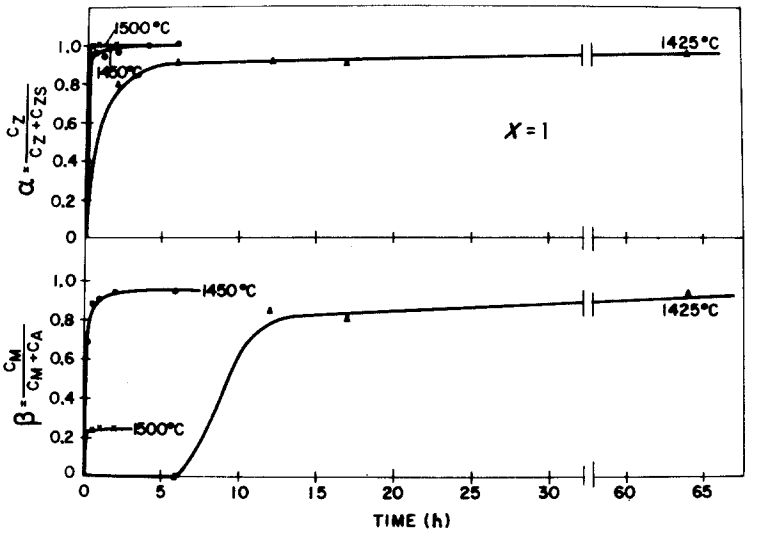

Figure 9 Reaction rate for $x = 1$ against time at different temperatures.

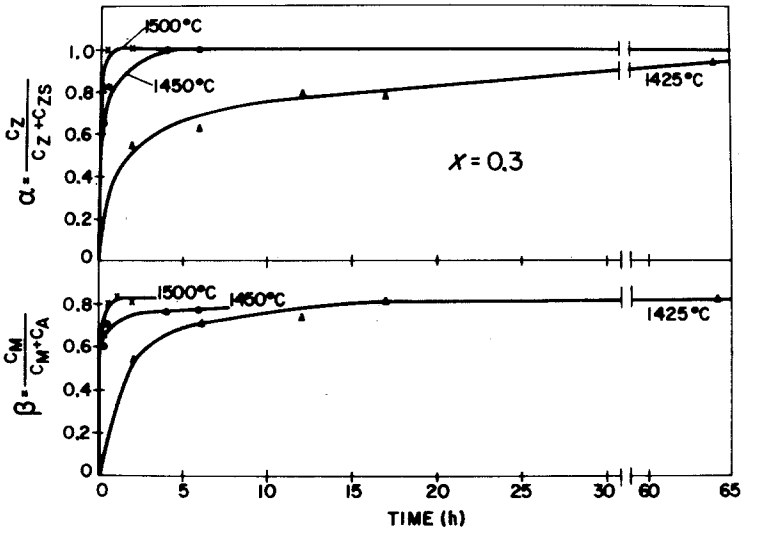

Figure 10 Reaction rate for $x = 0.3$ against time at different temperatures.

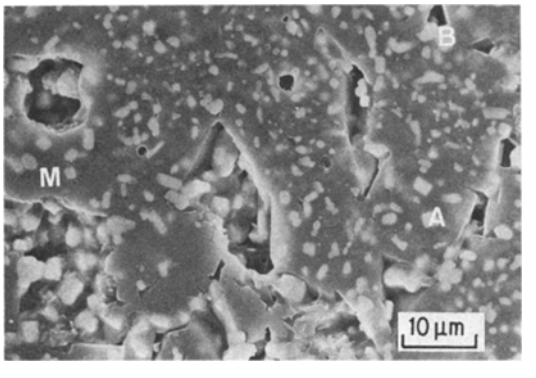

Figure 11 Microstructure of the sample with $x = 1$ treated for 1.5 h at 1450° C. A = zirconia intragranular, B = zirconia intergranular, M = mullite.

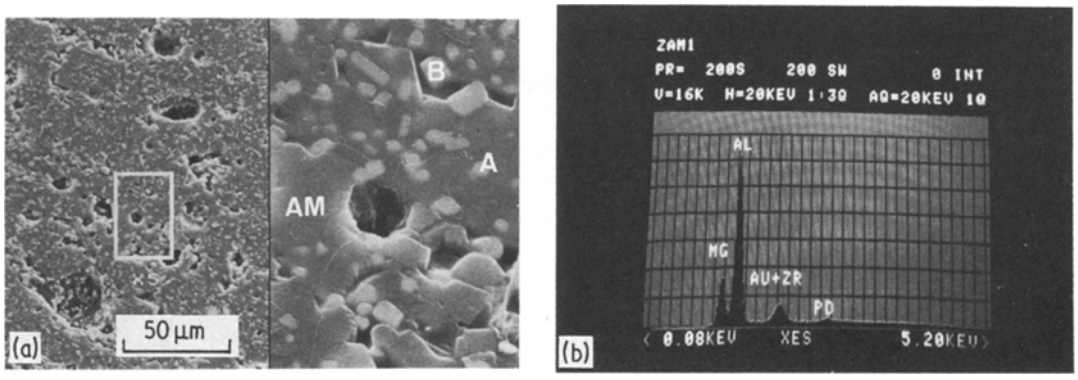

Figure 12 (a) Detail of the microstructure of the same sample showing a spinel grain, **AM** = Al_2MgO_4. (b) Aluminium and magnesium X-ray spectrum of the spinel grain.

generally, a round shape. The other one, *zirconia intergranular*, has sharp-edged grains located between mullite grain boundaries. This microstructure is similar to that mentioned before [1]. In this case the size of mullite grains is significantly greater (20 to 25 µm) and the number of intergranular particles is lower.

In this sample another phase, spinel, was observed to be located near small spherical pores (Fig. 12a); thus spinel growth, as an expansive phase, can be associated with the creation of porosity. It is interesting to notice that the spinel grains are essentially free of zirconia grains. This fact is explained because the formation of spinel takes place prior to zircon decomposition (Figs. 4 and 5).

In Fig. 12b the X-ray energy dispersion spectrum for the spinel grain of Fig. 12a is shown. In Fig. 13a a high-magnification micrograph of the same sample is shown. In this figure small (~ 1 µm) alumina grains, inside the mullite grain, have been identified by Kevex microanalysis (Fig. 13b).

Table I gives the mechanical properties as well as the relative tetragonal contents for the samples with $x = 1$ and $x = 0.3$, treated at different temperatures for different times. As before [1], the relative tetragonal content does not seem to influence the critical stress intensity factor.

The modulus of rupture was measured for the samples with the highest value of the critical intensity factor K_{IC}. The sample with $x = 0.3$ has a modulus of rupture higher than the sample with $x = 1$. This fact can be explained in the same way as in Part 1 [1], i.e. the sample with $x = 1$ has a relatively higher content of glass phase. As mentioned in Part 1 [1] a significant increase in K_{IC} and the bend strength σ_f was obtained in the MgO-containing samples.

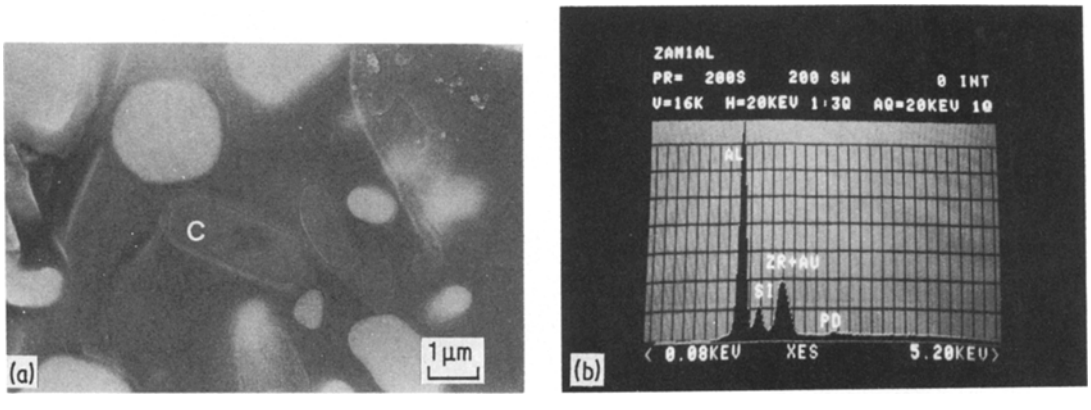

Figure 13 (a) High-magnification micrograph of the sample of Figure 12a. (b) Aluminium X-ray spectrum of an alumina grain. C = Al_2O_3.

TABLE I Properties of zircon/alumina/magnesia mixtures

Molar Composition*	T (° C)	Time (h)	X_t (%)	σ_f† (MPa)	K_{IC} (MPa $m^{1/2}$)
2 ZS/3 A/0.3 (A + M)†	1450	6	50	–	3.8
	1500	0.25	70	329 ± 8	4.6
	1500	1	55	–	4.5
2 ZS/3 A/ (A + M)	1425	67	8	–	3.39
	1450	6	16	–	3.4
	1450	1.5	21	258 ± 26	4.46

*ZS = $ZrSiO_4$ A = Al_2O_3 M = MgO
†Average value over five measurements

References

1. P. PENA, P. MIRANZO, J. S. MOYA and S. DE AZA, *J. Mater. Sci.* **20** (1985) 2011.
2. P. PENA, J. S. MOYA, S. DE AZA, E. CARDINAL, F. CAMBIER, C. LEBLUD and M. R. ANSEAU, *J. Mater. Sci. Lett.* **2** (1983) 772.
3. R. DAL MASCHIO, A. TIZIANI and I. CALLIARI, *Verres Réfract.* **37** (1983) 369.
4. C. BAUDIN and J. S. MOYA, *J. Amer. Ceram. Soc.*, **67** (1984) c-134.
5. D. NIN-KUO WANG, PhD thesis, University of California, Berkeley LBL-5763, 1983.
6. E. DI RUPO, M. R. ANSEAU and R. J. BROOK, *J. Mater. Sci.* **14** (1979) 2924.

Received 25 June
and accepted 6 July 1984